Bond-order wave phase, spin solitons and thermodynamics of a frustrated linear spin-1/2 Heisenberg antiferromagnet

Manoranjan Kumar[1,2], S. Ramasesha[2] and Z.G. Soos[1]
[1] *Department of Chemistry, Princeton University, Princeton NJ 08544 and*
[2] Solid *State and Structural Chemistry Unit, Indian Institute of Science, Bangalore 560012, India,*

(Dated: June 28, 2010)

The linear spin-1/2 Heisenberg antiferromagnet with exchanges J_1, J_2 between first and second neighbors has a bond-order wave (BOW) phase that starts at the fluid-dimer transition at $J_2/J_1 = 0.2411$ and is particularly simple at $J_2/J_1 = 1/2$. The BOW phase has a doubly degenerate singlet ground state, broken inversion symmetry and a finite energy gap E_m to the lowest triplet state. The interval $0.4 < J_2/J_1 < 1.0$ has large E_m and small finite size corrections. Exact solutions are presented up to $N = 28$ spins with either periodic or open boundary conditions and for thermodynamics up to $N = 18$. The elementary excitations of the BOW phase with large E_m are topological spin-1/2 solitons that separate BOWs with opposite phase in a regular array of spins. The molar spin susceptibility $\chi_M(T)$ is exponentially small for $T \ll E_m$ and increases nearly linearly with T to a broad maximum. J_1, J_2 spin chains approximate the magnetic properties of the BOW phase of Hubbard-type models and provide a starting point for modeling alkali-TCNQ salts.

PACS numbers: 71.10.Fd, 75.10.Pq, 75.60.Ch, 71.30.+h
Email: soos@princeton.edu

I. INTRODUCTION

The extended Hubbard model (EHM) has competing on-site repulsion $U > 0$, intersite interaction $V > 0$ and electron transfer t between neighbors in one dimension (1D) with evenly spaced sites. The half-filled case with one electron per site has several phases: a charge density wave (CDW) at $V > U/2$ with broken electron-hole symmetry and occupation numbers $n > 1$ on one sublattice, $n < 1$ on the other; a spin fluid phase at $V = 0$ as known from Hubbard models; and as proposed by Nakamura, [1] a bond-order wave (BOW) phase with broken inversion symmetry between the CDW and the spin fluid phases when t/U is sufficiently large for a continuous CDW transition. The BOW phase has long-range order and a finite magnetic gap E_m to the lowest triplet excited state. Multiple theoretical approaches,[2–5] primarily at $U \leq 2t$ and $U = 4t$, have confirmed a narrow BOW phase in the EHM. Other spin-independent potentials also support a BOW phase when the CDW transition is continuous [6]. The narrow BOW phase of Hubbard-type models presents major computational difficulties.

In this paper, we consider the BOW phase of a familiar spin-1/2 chain with frustrated antiferromagnetic (AF) exchange [7]. The BOW phase becomes numerically accessible and can be demonstrated in finite systems. Although charge fluctuations are strictly excluded in spin chains, the BOW phase again illustrates broken inversion symmetry at sites, long-range order and finite E_m. The spin chain has AF exchange between first and second neighbors,

$$H(x) = J \sum_n ((1-x)\vec{s}_n.\vec{s}_{n+1} + x\vec{s}_n.\vec{s}_{n+2}) \qquad (1)$$

We consider the interval $0 \leq x \leq 1$ and set the total exchange $J = 1$ as the unit of energy. The $x = 0$ limit is a linear Heisenberg antiferromagnet (HAF). Second-neighbor exchange $J_2 = xJ$ for $x > 0$ opposes short-range antiferromagnet (AF) order and eventually induces a fluid-dimer phase transition that has been the focus of recent studies [8–13]. The $x = 1$ limit gives two HAFs on the even and odd sublattice, respectively. White and Affleck [14] considered $J_2/J_1 > 1$ using field theory and the density matrix renormalization group (DMRG).

Okamoto and Nomura [8] located the transition at $x_c = x_1/(1-x_1) = 0.2411$, or $x_1 = 0.1943$ in our notation, where a magnetic gap E_m opens. The "dimer" phase refers to the earlier observation of Majumdar and Ghosh (MG) [7] that, for an even number N of spins and periodic boundary conditions (PBC), the exact ground state (gs) at $x_{MG} = 1/3$ ($J_2 = J_1/2$) has singlet-paired spins on adjacent sites, just as in the Kekulé diagrams shown in Fig. 1,

$$\begin{aligned} |K1\rangle &= (1,2)(3,4)...(N-1,N) \\ |K2\rangle &= (2,3)(4,5)...(N,1) \end{aligned} \qquad (2)$$

Kekulé diagrams are particularly simple BOWs. They illustrate broken inversion symmetry, long-range order, double degeneracy and finite excitation energies [10] at

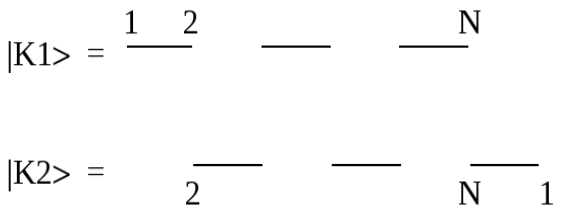

FIG. 1: Lines indicate singlet-paired spin on adjecent sites.

the MG point. Since these are the defining features of a BOW phase, that is what we will call the "dimer" phase. The notation $H(x)$ is convenient for the $x = 1$ limit of HAFs on the even and odd sublattices. Now $x < 1$ describes interchain exchange that is frustrated because each spin is coupled to two neighbors of the other sublattice. With constant total exchange, the gs energy is highest when the spin chain is the most frustrated.

For open boundary conditions (OBC), $|K1\rangle$ is the exact nondegenerate gs of $H(1/3)$. The chemical analogy is now to partial double and single bonds in linear polyenes or in polyacetylene. The BOW associated with $|K1\rangle$ is well understood in *dimerized* arrays whose elementary excitations are the topological solitons of the uncorrelated Su-Schrieffer-Heeger (SSH) model [15, 16]. Similar conclusions hold in correlated models of conjugated polymers [17] or ion-radical stacks [18]. Spin solitons in BOW systems at finite temperature separate $|K1\rangle$ and $|K2\rangle$ regions in infinite regular chains. The Peierls instability of Hubbard or spin chains is a separate topic that requires electron-phonon or spin-phonon coupling. Our discussion of $H(x)$ is limited to regular arrays with PBC or OBC.

To introduce the principal features of $H(x)$, we show in Fig. 2 the gs energy per site, $\epsilon_0(x)$, for intermediate $N \approx 20$ and PBC. Bonner and Fisher [19] found that $\epsilon_0(0)$ of the HAF converges as $\approx N^{-2}$ to the exact value, $-\ln 2 + 1/4$, due to Hulthen [20] and denoted by arrows at $x = 0$ and 1. Convergence at $x = 1$ is for two HAFs of $N/2$ sites, from below when $N/2$ is even and from above [21] when $N/2$ is odd. The shape of $\epsilon_0(x)$ indicates different frustration at small x for exchange J_2 in one HAF and at large x for exchange J_1 between two HAFs. Frustration is greatest at the $\epsilon_0(x)$ maximum. The Hellmann-Feynman theorem gives

$$\frac{\partial \epsilon_0(x)}{\partial x} = \frac{1}{N}\langle\psi_0(x)|\frac{\partial H}{\partial x}|\psi_0(x)\rangle = \frac{1}{N}\sum_n \langle(\vec{s}_n.\vec{s}_{n+2} - \vec{s}_n.\vec{s}_{n+1})\rangle \qquad (3)$$

The bond orders or spin correlation functions are equal at $\partial\epsilon_0/\partial x = 0$ when there is equal choice for pairing with a first or second neighbor. The slope $\partial\epsilon_0/\partial x$ is steeper

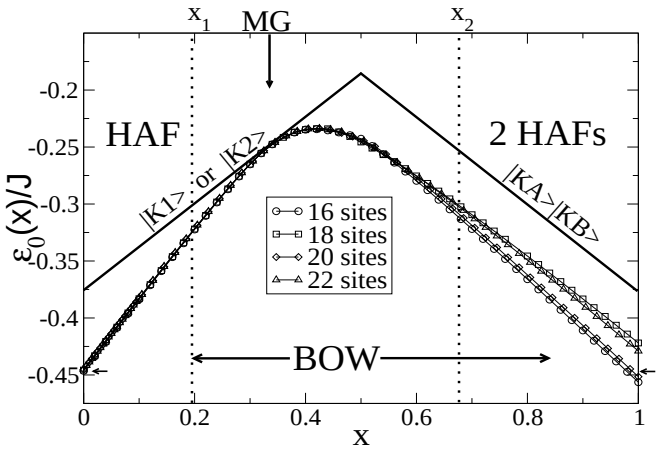

FIG. 2: Ground state energy per site, $\epsilon_0(x)$, of the spin chain $H(x)$ in Eq. 1 for N sites with periodic boundary conditions (PBC). The BOW phase starts at the fluid-dimer transition at x_1; x_2 is the excited state crossover discussed in the text. The energy of $|K1\rangle$ or $|K2\rangle$ in Eq. 2 is exact at $x_{MG} = 1/3$ and approximate for $x < 1/2$; the energy of a product of Kekulé diagrams $|KA\rangle|KB\rangle$ is approximate for $x > 1/2$. Arrows at $x = 0$ and 1 mark ϵ_0 of the infinite chain.

at $x = 0$ than at $x = 1$. First and second neighbor spin correlation functions are known [22] exactly at $x = 0$ and they add in Eq. 3. The slope at $x = 1$ is just the first-neighbor correlation function.

The solid lines in Fig. 2 are the energy of $|K1\rangle$ or $|K2\rangle$ for $x < 1/2$, exact at $x_{MG} = 1/3$, and of a product of Kekulé diagrams of two HAFs for $x > 1/2$. The BOW phase that we characterize below starts at x_1. We found $x_2 \approx 2/3$ using the Okamoto-Nomura [8] treatment of x_1. The gap E_m is exponentially small but finite for $x > x_2$, and the BOW phase extends to $x = 1$ according to White and Affleck [14].

The order parameter $B(x)$ is the gs amplitude of the BOW,

$$B(x) = \frac{1}{N}\sum_n (-1)^n \langle \vec{s}_n.\vec{s}_{n+1}\rangle \qquad (4)$$

The two gs have $\pm B(x)$. It follows immediately that $B(1/3) = 3/8$ for $|K1\rangle$ or $|K2\rangle$ in Eq. 2. As shown below, large $B(x)$ and $E_m(x)$ between $x = 1/3$ and $x \approx 1/2$ make possible our detailed finite-N study of the BOW phase.

The complete basis of $H(x)$ has dimension 2^N, since each spin-1/2 has two orientations, and the total spin $0 \le S \le N/2$ is conserved. Reflection σ through sites

corresponds to inversion symmetry C_i at sites in the infinite chain. Valence bond (VB) methods [23–26] are well suited for finite models that conserve S. A few states with any S and σ can be found exactly up to $N \approx 30$. The full spectrum is needed for thermodynamics and has been obtained [27] to $N = 16$, which we increase to $N = 18$. DMRG extends [28] thermodynamics to N = 64. The spin chain $H(x)$ benefits from the smaller basis compared to 4^N in Hubbard models with charge degrees of freedom. An even greater advantage may be the exact gs at the MG point for finite N. In contrast to the numerically difficult BOW phase of Hubbard-type models, the BOW phase of $H(x)$ is accessible to direct finite-N modeling between $x \approx 1/3$ and $x \approx 1/2$.

We characterize the gs properties of the BOW phase and its elementary excitations in Section II, including the magnetic gap $E_m(x)$, the order parameter $B(x)$, excited states at the MG point, and the bond-order domain walls of spin solitons. The temperature dependence of the molar spin susceptibility $\chi_M(T)$ and specific heat $C(T)$ are found in Second III. Following an activated regime that depends of E_m, $\chi_M(T)$ increases almost linearly with T in the BOW phase, quite differently from an HAF or an EHM with $t \ll (U - V)$. The Discussion relates $H(x)$ to the EHM and to π-radical salts with $\chi_M(T)$ nearly linear in T.

II. GROUND AND LOW-ENERGY STATES

We use valence bond (VB) methods [25, 26] to solve $H(x)$ exactly for finite N and either periodic or open boundary conditions in exact subspaces with fixed total S and reflection $\sigma = \pm 1$ at sites. The gs is a singlet, $S = 0$, with either $\sigma = 1$ or -1 depending on N and x. The linear combinations $|K1\rangle \pm |K2\rangle$ in Eq. 2 transform as $\sigma = \pm 1$, even or odd under inversion in the infinite chain. The gs for other x is a symmetry adapted linear combination of singlet VB diagrams $|k\rangle$. We define $E_\sigma(x)$ as the excitation energy to the lowest singlet with opposite σ symmetry. Figure 3 compares $E_\sigma(x)$ for $N = 24$ and PBC to the gap $E_m(x)$ to the lowest triplet. Finite-size effects are large at $x = 0$ for an HAF of 24 sites and about twice as large at $x = 1$ for two HAFs of 12 sites, as expected when excitations energies go as $\approx 1/N$. We obtained similar graphs of $E_\sigma(x)$ and $E_m(x)$ up to $N = 28$. There is no difference at small x aside from $1/N$ effects. The excitations are qualitatively different at $x \approx 1$, however, when $N/2$ is even or odd. Even $N/2$ is required for proper comparison at $x = 0$ and 1. When $N/2$ is odd, the $x = 1$ limit corresponds to two HAFs with an odd number of spins and a doublet gs. Since the radical also has two-fold orbital degeneracy [21], there are several gapless excitations in the $x = 1$ limit of no interchain exchange.

Okamoto and Nomura [8] identified the quantum transition at x_1 by finding $E_\sigma(x_1) = E_m(x_1)$ from N = 10 to 24. They argued that an excitation crossover at finite N is more accurate than extrapolation to find $E_m(x_1) = 0$. The slow variation of $x_1(N)$ and extrapolations made possible their accurate determination of x_1. Our results for $x_1(N)$ in Table 1 to $N = 24$ agree with ref. 8. Previous work [8–13] focused on the fluid-dimer transition at x_1, while we are interested in the BOW phase with $x > x_1$. The same method yields $E_m = E_\sigma$ at $x_2(N)$ in Table I for even and odd $N/2$. Finite-size effects are stronger because the chains are effectively half as long. A joint $1/N$ extrapolation of the two sequences returns $x_2 = 0.67 \pm 0.01$ ($J_2/J_1 = 2.03 \pm 0.03$). The x_2 crossover does not signify the termination of BOW phase, however, which extends [14] to $x = 1$. We improved the accuracy of the DMRG algorithm [29] to look at $x > x_2$ and find small but finite $E_m(x)$ and $B(x)$ up to $x = 0.8$ ($J_2/J_1 = 4.0$), beyond which even more accurate DMRG is required. We do not understand the different implication of x_1 and x_2 crossovers, but note that $H(x)$ also has a spiral phase [30] starting at $x_{MG} = 1/3$ whose order parameter is twist angle. In the present work we focus on the BOW phase with large $B(x)$ and $E_m(x)$.

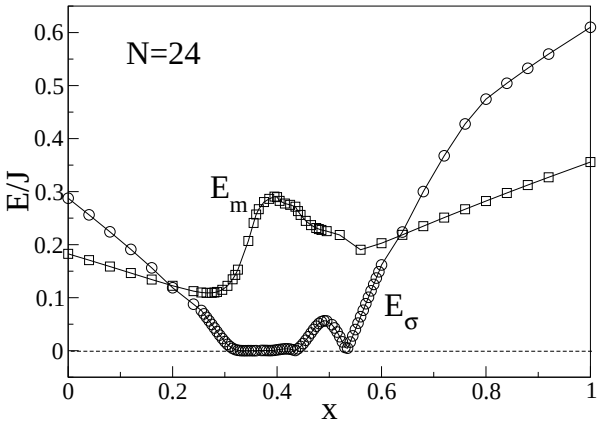

FIG. 3: Finite-size effects on excitation energies of $H(x)$ for $N = 24$ with PBC. E_m is the excitation to the lowest triplet and E_σ to the lowest singlet with opposite inversion symmetry. The crossovers $x_1(24)$ and $x_2(24)$ are listed in Table I.

The BOW phase of the extended system has degenerate gs in the $\sigma = \pm 1$ sectors and hence $E_\sigma(x) = 0$. Finite-size effects are extraordinarily small for $0.3 < x < 0.5$ where E_0 is close to $-N/4$. The difference in *total* energy, $E_0(x, 1) - E_0(x, -1)$, for $\sigma = \pm 1$ is shown in Fig. 4 up to $N = 30$. The absolute gs for $x < 1/3$ is $E_0(-1)$ for $N = 4p$ and $E_0(1)$ for $N = 4p + 2$. The $E_0(x, \pm 1)$ curves are degenerate at $x = 1/3$ without crossing. They cross for $x > 1/3$ and the number of crossings depends on N.

TABLE I: Crossing points $x_1(N)$ and $x_2(N)$ where $E_m(x) = E_\sigma(x)$ for N sites and PBC.

N	x_1	x_2 ($N/2$ odd)	x_2 ($N/2$ even)
18	0.1949	0.5669	
20	0.1947		0.6262
22	0.1947	0.5784	
24	0.1946		0.6368
26	0.1946	0.5885	
28	0.1944		0.6421
∞	0.1943 [a]	0.68	0.66

[a] ref.8

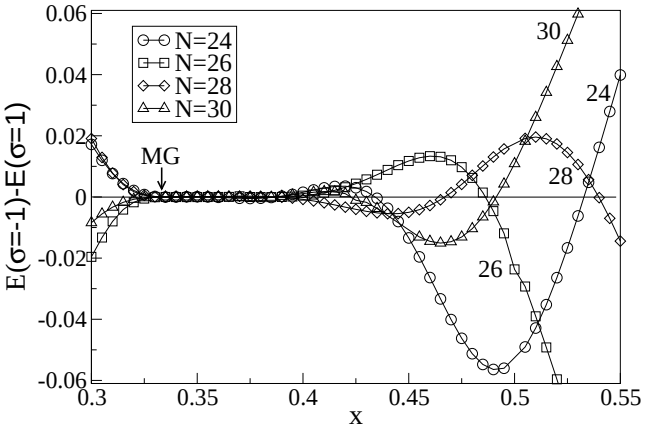

FIG. 4: Finite-size effects on the energy the lowest singlets of $H(x)$ with opposite inversion symmetry in the BOW phase. The energies are equal at $x = 1/3$ without crossing. Crossings at $x > 1/3$ are governed by the ground-state symmetry at $x = 0$ and 1 as discussed in the text.

When $N = 4p$ and p is even, the gs at $x = 1$ also transforms as $\sigma = -1$; there is an even number of crossings for $N = 24$ or 16. The E_σ bump in Fig. 3 at $x = 0.5$ is due to two crossings. For $N = 4p$ and odd p, the $x = 1$ gs has $\sigma = 1$ symmetry that requires an odd number of crossings for $N = 28$ or 20. The gs for $N = 4p + 2$ has $\sigma = 1$ symmetry for $x < 1/3$. There is an even number of crossings up to $x = 0.60$ for $N = 26$ or 18 (even p) and an odd number for N = 30 or 22 (odd p). Degeneracy without crossing at the MG point and subsequent symmetry crossovers for finite N are the principal reasons for remarkably small $E_\sigma(x)$ in this interval.

Since $E_\sigma(N) > 0$ is due to finite-size effects in the BOW phase, extrapolation of $E_m(N) - E_\sigma(N)$ yields $E_m(x)$. As seen in Fig. 5, $E_m(N) - E_\sigma(N)$ converges well to $E_m(x)$ on the x_1 side and less well on the x_2 side where even and odd $N/2$ appear for $x_2(N)$ in Table I. The largest magnetic gap is $0.29J$ at $x = 0.40$, close to the $\epsilon_0(x)$ peak in Fig. 2 and clearly beyond $x_{MG} = 1/3$.

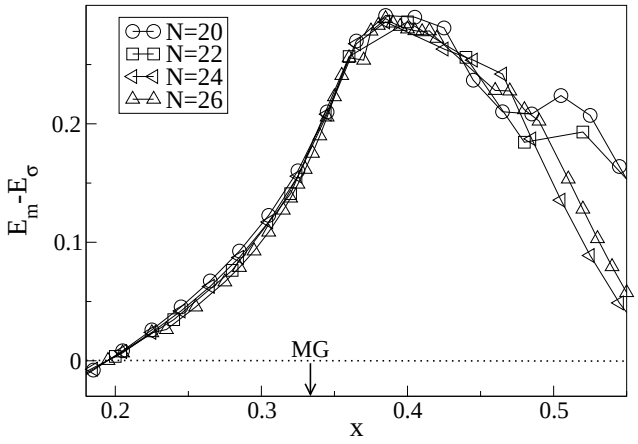

FIG. 5: Excitation energy $E_m(x)$ to the lowest triplet of $H(x)$ for finite N and PBC in the BOW phase. The infinite chain has $E_\sigma(x) = 0$ and a doubly degenerate ground state.

The E_m maximum and position agree well with DMRG in Fig. 5 of ref. 14. Since Fig. 4 shows $E_\sigma(x)$ to be very small between $x = 0.3$ and 0.5, large E_m in this interval is consistent with small finite-size corrections. More accurate DMRG is needed [29] for $E_m(x)$ at $x > 0.5$.

To obtain the BOW amplitude $B(x)$, we break inversion symmetry according to

$$H(x, \delta) = H(x) + \delta \sum_n (-1)^n \vec{s}_n . \vec{s}_{n+1} \qquad (5)$$

At the MG point, $|K1\rangle$ is the gs for $\delta = 0+$ and $|K2\rangle$ for $\delta = 0-$. The gs energy per site, $\epsilon_0(x, \delta)$, gives $B(x) = -(\partial\epsilon_0/\partial\delta)_0$. The inset of Fig. 6 shows $-(\epsilon(1/3, \delta) - \epsilon(1/3, 0))/\delta$ for $N = 20$ as a function of δ. The intercept is $B(1/3) = 3/8$ while the slope is $\chi_d/2$, the harmonic electronic force constant per site for dimerization that will be needed in a later study of lattice vibrations. Fig. 6 shows $B(x)$ in the BOW phase. $B(1/3) = 3/8$ follows directly from $-\langle \vec{s}_n . \vec{s}_{n+1} \rangle = 3/4$ or 0 for paired and unpaired neighbors, respectively. The N dependence of $B(x)$ is negligible near the MG point up to $x \approx 0.45$, but it becomes significant around $x \approx 0.5$ where the location of the gs crossings in Fig. 4 depend on N. Finite-size effects also appear near x_1 and x_2 where $B(x)$ becomes small but does not vanish. Since $\psi_0(x', \pm)$ with $\sigma = \pm 1$ are degenerate at crossings x', the linear combinations $(\psi_0(x', +) \pm \psi_0(x', -))/\sqrt{2}$ are broken-symmetry states whose expectation value in Eq. 4 leads to

$$B(x') = |\langle \psi_0(x', +)| \sum_n (-1)^n \vec{s}_n . \vec{s}_{n+1} |\psi_0(x', -)\rangle|/N \qquad (6)$$

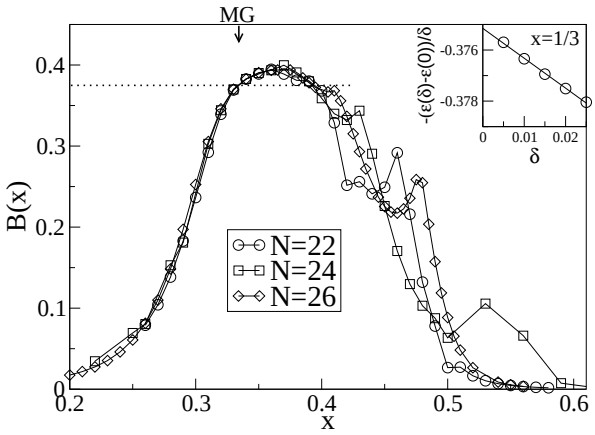

FIG. 6: Amplitude $B(x)$ in Eq. 4 of the BOW of $H(x)$ for finite N and PBC in the BOW phase. $B(1/3) = 3/8$ is exact for either $|K1\rangle$ or $|K2\rangle$ in Eq. 2. Finite-size effects around $x \approx 1/2$ are due to reversals of the ground states inversion symmetry. The inset shows $-[\epsilon_0(1/3,\delta) - \epsilon_0(1/3)]/\delta$ vs δ at $N = 20$ for the symmetry-breaking perturbation in Eq. 5.

The matrix element agrees quantitatively with $B(x') = -(\partial\epsilon_0(x',\delta)/\partial\delta)_0$, as it must. The two determinations of $B(x)$ are the same within our numerical accuracy when $E_\sigma < 0.01J$.

To our surprise, $B(0.35)$ is slightly but distinctly larger than 3/8, the amplitude at the MG point for $|K1\rangle$ or $|K2\rangle$. A Kekulé diagram has perfect AF correlation with one neighbor, which seems to be the limiting case of a BOW. While the AF correlation or bond order decreases slightly in systems with $B(x) > 3/8$, there is now small F correlation or negative bond order with the other neighbor. Direct solution of systems with OBC and $B(x) > 3/8$ yields large positive and small negative bond orders that alternate along the chain. We recall that the second-neighbor bond orders, $-\langle\vec{s}_n.\vec{s}_{n+2}\rangle$, are negative for $x < 1/3$, vanish at $x = 1/3$, and are positive for $x > 1/3$. The BOW phase for $x > 1/3$ has AF correlations for second neighbors and alternating strong AF and weak F correlations for first neighbors. We also note that $B(x)$ and $E_m(x)$ are not simply proportional to each other. The $B(x)$ maximum in Fig. 6 is at decisively lower x than the $E_m(x)$ maximum in Fig. 5. White and Affleck [14] were also surprised that $d = 2B$ could exceed 3/4 at $J_2/J_1 > 1/2$ and interpreted the result as ferromagnetic correlation; Fig. 8 of ref. 14 agrees quantitatively with Fig. 6 for $0.3 < x < 0.5$.

We consider next the excited states of $H(x)$ and present results at $x_{MG} = 1/3$ that are representative for the interval $0.3 < x < 0.5$ in which $B(x)$ and $E_m(x)$ are large. The gs energy per site at the MG point is $\epsilon_0(1/3) = -1/4$ for either PBC or OBC. Table II list excitations with increasing energy for $N = 24$, 26 and 28. Sparse matrix methods [25, 26] are used for a few states in each symmetry subspace. It becomes progressively more difficult numerically to go beyond 3 or 4 states for large N. The notation Sr indicates total spin S and state index, $r = 1, 2, 3....$ States are doubly degenerate with wavevector $\pm k$ except for $k = 0(\sigma = +1)$ and $\pi(\sigma = -1)$. The lowest triplet at E_m and singlet at E_3 decrease slowly with N and are known rigorously to be finite in the infinite chain [10]. Finite-size effects are more pronounced with increasing r. The gap $E_3 - E_m$ decreases with N. We expect it to vanish in the extended system whose elementary excitation are spin solitons, each with $s = 1/2$, with paired or parallel spins. There are additional singlets and triplets below the lowest quintet at $E_Q(N)$.

TABLE II: Excitation energies $E(Sr)$ of $H(1/3)$, in units of J, for N sites and PBC.

Spin and State, Sr	N=28	N=26	N=24
Triplet, T1	0.1691	0.1705	0.1727
Singlet, S3	0.1757	0.1793	0.1839
T2, T3	0.1833	0.1873	0.1921
S4, S5	0.1898	0.1953	0.2022
T4	0.2089	0.2155	0.2242
Quintet, Q1	0.4200	0.4324	0.4499

Since all sites of $H(x)$ are equivalent for PBC, it is difficult to discern solitons even with exact eigenstates in hand. Fortunately, the gs energy per site for OBC and even N is again $\epsilon_0 = -1/4$, and the gs $|K1\rangle$ in Fig. 1 has alternating bond orders of 3/4 and 0 along the chain. We consider $H(1/3)$ with OBC and odd N, either $N = 4p + 1$ or $N = 4p - 1$. The gs is a doublet, $S = S^z = 1/2$, with spin density $\rho_n = 2\langle S^z_n\rangle$ at site n. With central site at $n = 0$, the terminal sites are $\pm 2p$ when $N = 4p + 1$ and $\pm 2(p - 1)$ when $N = 4p - 1$. Linear polyenes or VB diagrams rationalize two distinct series when N is finite. The pentyl radical ($N = 5$) has $\rho_0 > 0$ and partial single bonds at the center, while the allyl radical ($N = 3$) has $\rho_0 < 0$ and partial double bonds at the center. Soliton spin densities of $H(1/3)$ for $N = 25$ and 23 are shown in Fig. 7. Sites with $\rho < 0$ indicate electronic correlation [31] and correspond to nodes in uncorrelated Hückel or tight-binding theory.

The gs bond orders of $H(1/3)$ for odd N are close to 3/4 at the end and reverse in between. The $(N - 1)/2$ bond orders are symmetric about the center, $n = 0$. Fig. 8 displays $-\langle\vec{s}_n.\vec{s}_{n+1}\rangle$ for different values of N. Bond orders oscillate with increasing n and grow from the center. As expected, the central bond order is slightly larger for the $4p-1$ series than for the $4p+1$ series. Both spin densities and bond orders are typical of spin-1/2 solitons that for $H(1/3)$ connect $|K1\rangle$ and $|K2\rangle$ regions. In a BOW phase, broken inversion symmetry and solitons are found in regular arrays. Of course, the soliton width

2ξ depends on models and parameters; 2ξ increases with decreasing dimerization in the SSH model [15] and it also depends on correlations. The results in Figs. 7 and 8 suggest that spin solitons at the MG point have $2\xi \approx 15$.

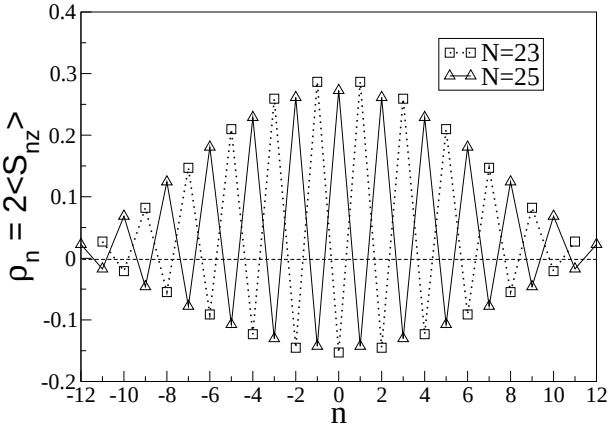

FIG. 7: Spin densities $\rho_n = 2\langle S^z_n\rangle$ in the doublet ground state of $H(1/3)$ with OBC and $N = 23$ and 25. The central site at $n = 0$ has large positive ρ_0 for $N = 25$ and small negative ρ_0 for N = 23, as discussed in the text. The spin soliton is delocalized over the central part in either case.

The energy $2E_W$ of two domain walls is found by comparing the gs energy of even and odd systems with OBC and equal length,

$$2E_W(x,N) = 2E_0(x,N) - E_0(x,N-1) - E_0(x,N+1) \quad (7)$$

At the MG point, we find $2E_W$= 0.1701, 0.1684 and 0.1669 for N =23, 25 and 27, respectively, slightly less than the E_m values in Table II for even N. $2E_W(1/3,N)$ has weaker N dependence than $E_m(1/3,N)$, and a joint extrapolation returns $2E_W = E_m = 0.151$ for the infinite chain. Finite-size effects are larger for $E_3(1/3,N)$ in Table II and even larger for $E_Q(1/3,N)$.

Direct solution up to $N \approx 30$ indicates that the elementary excitations of $H(1/3)$ are spin-1/2 solitions with $2E_w = E_m = E_3 = E_Q/2$ in the infinite chain. Finite N results suffice for $0.3 < x < 0.5$ when $B(x)$ and $E_m(x)$ are large. Longer chains can be studied using DMRG methods that will be needed for the BOW phase of Hubbard-type models. Since 1D systems at $T > 0$ cannot have long-range order, topological solitons are generic features of systems with a BOW phase. The present discussion is limited to a rigid lattice with purely electronic domain walls, but solitons are also expected in deformable lattices with linear electron- or spin-phonon coupling.

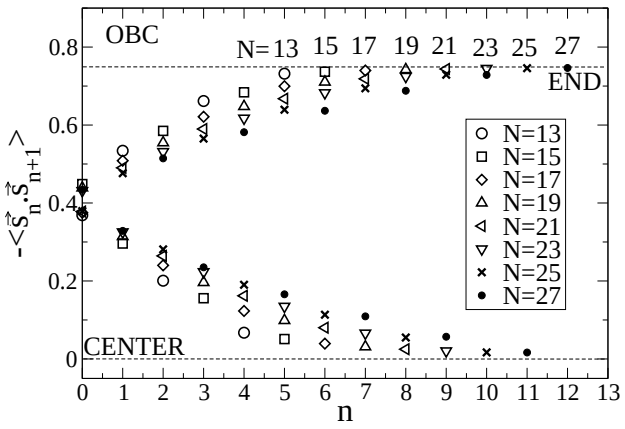

FIG. 8: Ground-state bond orders, $-\langle\vec{s}_n.\vec{s}_{n+1}\rangle$ of $H(1/3)$, for odd N and open boundary conditions (OBC). The bond orders are symmetric about the center, $n = 0$, and increase to almost 3/4 at the ends.

III. MAGNETIC SUSCEPTIBILITY AND SPECIFIC HEAT

Static magnetic susceptibility provides by far the most direct comparison with experiment, as amply illustrated [32, 33] by Heisenberg and other spin chains and by spin-Peierls systems. The molar spin susceptibility, $\chi_M(T)$, is an absolute comparison for organic radicals with small spin-orbit coupling and g close to 2.00236, the free-electron value. Since $H(x)$ conserves S, the energy level E_{Sr} splits into $2S+1$ Zeeman levels in an applied field. The full energy spectrum of $H(x)$ in zero field is required to construct the partition function

$$Q_N = \sum_{S=0}^{N/2}\sum_r (2S+1)\exp(-E_{Sr}/k_BT) \quad (8)$$

where k_B is the Boltzmann constant and E_{Sr} is excitation energy from the singlet gs to the r^{th} energy level with spin S. The molar spin susceptibility of an N-site chain is [27]

$$\chi_M(T,N) = \frac{N_A g^2\mu_B^2}{3k_BTNQ_N}\sum_{S=0}^{N/2}\sum_r S(S+1)\times (2S+1)\exp(-E_{Sr}/k_BT) \quad (9)$$

where N_A is Avogadro's number and μ_B is the Bohr magneton. Finite-size effects become severe when k_BT is small compared to $E_m(N)$.

Fig. 9 shows χ_M for N = 16 as a function of k_BT/J for several values of x. The curves converge for $T > J/k_B$

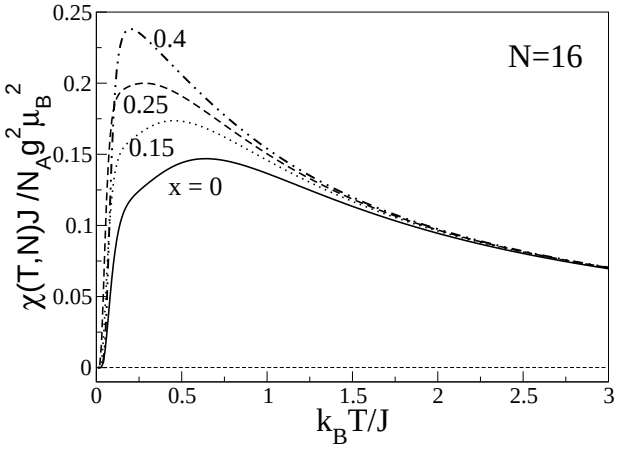

FIG. 9: Molar spin susceptibility, $\chi_M(T,N)$ in Eq. (10), vs k_BT/J for spin chains with $N = 16$ and PBC for $x = 0$, 0.15, 0.25 and 0.40 in Eq. (1). The fluid phase up to $x_1 = 0.1943$ has finite $\chi_M(0)$. The curves become independent of x at high T.

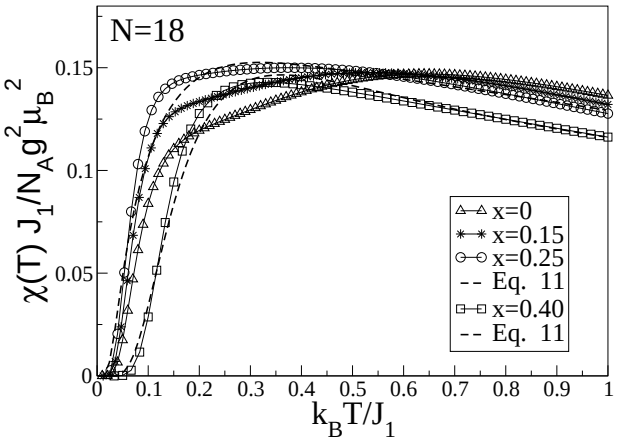

FIG. 10: Molar susceptibility, $\chi_M(T,N)$ in Eq. 9, vs k_BT/J_1, the nearest-neighbor exchange, for spin chains with $N = 18$ and PBC. The dashed lines for $x = 0.25$ and 0.40 are Eq. 11 with parameter shown in Fig. 11.

because the total number of spins is the same and so is the Weiss constant $J/2k_B$. The number of spins and Weiss constant are the T^{-1} and T^{-2} terms, respectively, at high T. The $\chi_M(T)$ maxima are well converged at $N = 16$, as can be shown by solving $N = 18$ or 14. The situation is different as $T \to 0$, where $x < x_1$ leads to finite $\chi_M(0)$ in the fluid phase [8] while $x > x_1$ has $\chi_M(0) = 0$ due to finite E_m. The $x = 0$ and 0.15 curves for finite N are dominated by finite-size effects at low enough T. The $x = 0.40$ curve is almost quantitative since $E_m(0.4)$ exceeds zero-field effects at $N = 16$. The $x = 0.25$ curve is intermediate since E_m is finite but N dependent.

For reasons given in the Discussion, we are interested in variable $J_2 = xJ$ at constant $J_1 = J(1-x)$. The $\chi_M(T)J_1$ maxima in Fig. 10 depend weakly on J_2 up to $x = 0.40$; the curves now cross because the Weiss constant varies with x. The HAF ($x = 0$) maximum broadens and shifts to lower T with increasing $J_2/J_1 = x/(1-x)$. Size convergence at low T is shown in Fig. 11 for $x = 0.25(J_2/J_1 = 1/3)$ and $x = 0.40$ ($J_2/J_1 = 2/3$). Large E_m at $x = 0.40$ gives convergence at N=16 and 18. Small E_m at $x = 0.25$ limits convergence to the broad $\chi_M(T)$ maximum. In either case, finite E_m ensures that $\chi_M(0) = 0$ and gives a substantial range in which $\chi_M(T)$ is almost linear in T. The slope of the linear regime depends weakly on N.

There are many realizations of dimerized HAFs with $x = 0$ in Eq. 1 and alternating $J(1 \pm \delta)$ along the spin chain [32, 34]. Dimerized chains with $\delta > 0.3$ are well approximated as $N/2$ singlet-triplet (ST) pairs with spin-wave dispersion [34, 35]. An ST approximation also provides insight into the BOW phase. A normalized density $n(E)$ of two-level systems with ST gap E leads to

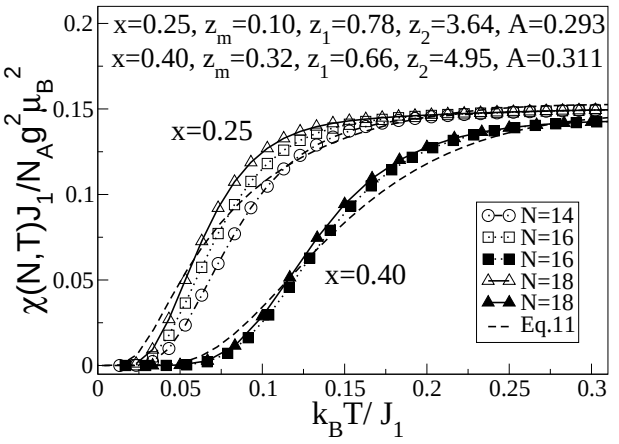

FIG. 11: Finite-size effects on $\chi_M(T,N)$ in the BOW phase of $H(x)$ at $x = 0.25$ and 0.40. Large $E_m(0.40)$ gives small changes for $N = 16$ and 18, while small $E_m(0.25)$ leads to stronger N dependence. The dashed lines for $x = 0.25$ and 0.40 are Eq. 11 with the indicated parameters z_i and A.

$$\chi_{ST}(T) = \frac{N_A g^2 \mu_B^2}{k_B T} \int_0^\infty \frac{n(E)dE}{\left(3 + \exp(E/k_BT)\right)} \qquad (10)$$

The integral can be evaluated for any piecewise constant $n(E)$. We consider $n(E) = 0$ aside from two intervals; $n(E) = A/(E_1 - E_m)$ for $E_m \le E \le E_1$ and $n(E) = (1-A)/(E_2 - E_1)$ for $E_1 \le E \le E_2$. The molar susceptibility is

$$\frac{\chi_{ST}(T,N)J_1}{N_A g^2 \mu_B^2} = \frac{A}{3(z_1 - z_m)} \ln\left(\frac{1+3\exp(-z_m J_1 k_B T)}{1+3\exp(-z_1 J_1 k_B T)}\right) + \frac{1-A}{3(z_1 - z_2)} \times \ln\left(\frac{1+3\exp(-z_1 J_1 k_B T)}{1+3\exp(-z_2 J_1 k_B T)}\right) \quad (11)$$

with $z_m = E_m J_1$, $z_1 = E_1 J_1$ and $z_2 = E_2 J_1$. As expected, the ST gap gives an exponential χ_{ST} at sufficiently low T, thereby fixing z_m. The width of $n(E)$ is controlled by z_2 and is fixed by the $\chi_M(T)$ maximum. The shape of $\chi_{ST}(T)$ can be varied by A and z_1, or by additional parameters when $n(E)$ has more than two intervals. The dashed lines in Figs. 10 and 11 are $\chi_{ST}(T)$ with the parameters in Fig 11. The spin susceptibility in the BOW phase is reasonably well modeled with a distribution $n(E)$ of ST gaps that is constant in two intervals.

The molar specific heat of $H(x)$ for N sites is

$$\frac{C(T)}{N_A k_B} = \frac{1}{N}\left(\frac{J}{k_B T}\right)^2 (\langle E(T)^2\rangle - \langle E(T)\rangle^2) \quad (12)$$

The thermal averages require the energy spectrum E_{Sr} and degeneracy. The results below are for PBC. Since S is conserved, separate contributions to $\langle E(T)\rangle$ can readily be identified. But the entropy is not additive in S and there is no unique partitioning of $C(T)dT = TdS$ into contributions in S. One choice is the temperature derivative of the S component of $\langle E(T)\rangle$. Another choice is based on fluctuations,

$$\frac{C(T)}{N_A k_B} = \frac{1}{NQ_N}\left(\frac{J}{k_B T}\right)^2 \sum_{Sr}(2S+1) \times (E_{Sr} - \langle E\rangle)^2 \exp(-E_{Sr}/k_B T) \quad (13)$$

with $C_S(T)$ given by the sum over r for fixed S. The $C_S(T)$ contributions in Eq. 13 are manifestly positive and are shown below. We also decomposed $C(T)$ based on $\langle E(T)\rangle$. The results are similar at low T, the region of interest.

Fig. 12 shows $C(T,x)$ at $x = 0.25$ and 0.40 as a function of $k_B T/J_1$ for $N = 18$. The contributions of $S = 0$, 1 and of $2 \le S \le 9$ are indicated with dashed lines. Large E_m at $x = 0.40$ gives a $C(T)$ peak due to $S = 0$, 1 and a shoulder at higher T for $S \ge 2$ contributions that start with $E_Q \approx 2E_m$. Small E_m at $x = 0.25$ gives a single broad $C(T)$ peak whose maximum shifts smoothly to higher $k_B T/J_1$ in the fluid phase with $x < x_1$. Likewise, there is a single $C(T)$ peak when E_m becomes small for $x > 0.5$. Finite E_m in the BOW phase shifts the singlet and triplet part of $C(T)$ to low energy and separates them from $S \ge 2$ contributions.

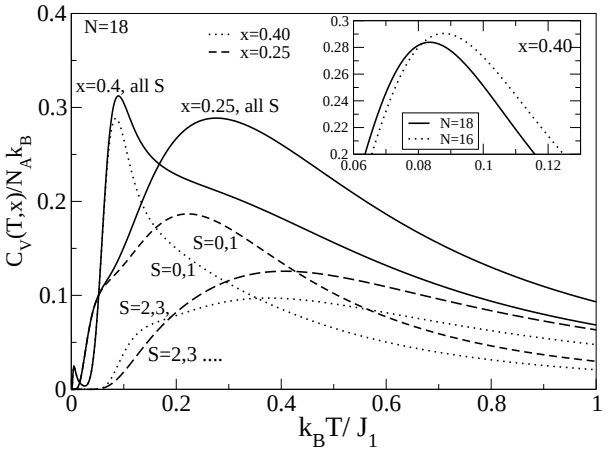

FIG. 12: Molar specific heat $C(T)$ in Eq. 13 in the BOW phase of $H(x)$ at $x = 0.25$ and 0.40 for $N = 18$ and PBC. The dotted and dashed lines are contributions in $S = 0{,}1$ and $S \ge 2$, respectively, according to Eq. 13. The inset shows the $S = 0{,}1$ contribution for $x = 0.40$ at $N = 16$ and 18.

Mütter and Wielath [36] reported $C(T)$ results for $8 \le N \le 16$ using a different numerical procedure and without resolving contributions in S. Their $C(T)$ and $\chi_M(T)$ curves are quite similar to ours, but not identical. In particular, their $C(T, 1/3)$ develops a shallow minimum at $N = 16$ that we do not see at either $N = 16$ or 18. Without proposing an explanation for the $C(T, 1/3)$ maxima, Mütter and Wielath [36] interpreted the discontinuity of the $C(T,x)$ maximum at the MG point as a transition from a "dimer" to a "frustrated" phase that, moreover, survived in the limit of large N. On the contrary, our results indicate a single phase for $x > x_1$ and we understand the $C(T)$ curves in Fig. 12 in terms of $S = 0$, 1 and $S \ge 2$ contributions. We turn next to $C(T)$ at large $N = 2n$. The fraction of singlets among the 2^{2n} spin states is

$$f_0(2n) = \frac{(2n)!2^{-2n}}{n!(n+1)!} \approx \frac{(n+1)^{-\frac{3}{2}}}{\sqrt{\pi}} \frac{e}{(1+\frac{1}{n})^n} \quad (14)$$

The second expression follows from Stirling's approximation and is accurate to within a few percent for $2n = 16$ or 18. The triplet fraction is $9nf_0/(n+2)$. Since f_0 decreases as $(2/N)^{-3/2}$, the $C(T)$ contribution from $S = 0$ and 1 becomes negligible compared to $S \ge 2$ in the thermodynamic limit. The inset in Fig. 12 compares the

$S = 0$, 1 maxima for $N = 16$ and 18. The N = 18 maximum is lower as expected for Eq. 14. The DMRG results of Feiguin and White [28] for $C(T, 1/3)$ at $N = 32$ and 64 show a small shoulder at low T that they attribute to finite-size effects.

IV. DISCUSSION

We have characterized the BOW phase of the linear spin-1/2 chain, $H(x)$ in Eq. 1, with frustrated Heisenberg AF exchange $J_1 = J(1-x)$ between neighbors and $J_2 = Jx$ between second neighbors. Exact VB methods yield the energies and eigenstates of finite systems with periodic or open boundary conditions. The BOW phase for $x > x_1 = 0.1943$ has a broken C_i symmetry and finite magnetic gap $E_m(x)$. Our results are most accurate for $0.3 < x < 0.5$ where large $E_m(x)$ ensures small finite-size corrections. Larger N, DMRG or other methods will be needed to characterize the BOW phase with small $E_m(x)$ or $B(x)$ at $x > 0.5$.

The BOW phase is particularly simple at $x = 1/3$, the MG point, where the exact gs for PBC is either Kekulé diagram $|K1\rangle$ or $|K2\rangle$ in Fig. 1, and $|K1\rangle$ for OBC. The BOW amplitude is $B(x)$ in Eq. 4, with $B(1/3) = 3/8$ and a broad maximum in Fig. 6 at lower x than the $E_m(x)$ maximum in Fig. 5. Topological spin-1/2 solitons that reverse the bond order are the elementary excitations of the BOW phase, as shown in Fig. 7 and 8 at $x = 1/3$ for odd N and OBC. The energy $2E_W$ of two solitons corresponds for finite N to E_m for parallel spins or to E_3 for paired spins. We have also found the consequences of finite $E_m(x)$ on the molar spin susceptibility $\chi_M(T)$ and specific heat $C(T)$.

The magnetic properties of the EHM with parameters U, V and t are closely related to $H(x)$ when $t \gg (U-V)$. Van Dongen [37] mapped the EHM in the spin sector to $H(x)$ with

$$\begin{aligned} J(1-x) \equiv J_1 &= \frac{4t^2}{U-V} + 4J_2 \\ xJ \equiv J_2 &= \frac{4t^4}{(U-V)^3} \end{aligned} \qquad (15)$$

The HAF is the familiar limit $t \ll (U-V)$ leading to $x = 0$. Increasing V at constant t and U amounts to increasing $J_2/J_1 = x/(1-x)$. The CDW transition of the EHM is close to $V = U/2$. Since a continuous CDW transition [3, 4] requires $t > U/7$, the $t \ll (U-V)$ approximation fails at the BOW boundary of the EHM. The next term goes as t^6 and in addition to J_1, J_2 contributions, it adds [38] a four-spin contribution that requires going beyond $H(x)$. Charge degrees of freedom cannot be neglected in the BOW phase of the EHM or of related models with Coulomb interactions.

It is nevertheless attractive to approximate magnetic properties of Hubbard-type BOWs with $H(x)$, much as HAFs have been used for Hubbard models. Finite E_m implies an exponentially small $\chi_M(T)$ at low T followed by a roughly linear increase up to 0.15 in reduced units. As seen Figs. 10 and 11, the χ_M maximum depends weakly on J_2. Linear $\chi_M(T)$ vs T behavior is distinctly different from an HAF [35] or a Hubbard model [39] with $E_m = 0$ and finite $\chi_M(0)$ that exceeds 60% of the χ_M maximum. Linear $\chi_M(T)$ following an onset has been observed [40] in several alkali-TCNQ salts up to $T \approx 450K$, the limit of their thermal stability. In our opinion, such $\chi_M(T)$ in regular arrays are signatures of BOW phases with $E_m > 0$ in Hubbard-type models as well as in $H(x)$.

There are several reasons for considering 1:1 alkali-TCNQ salts as possible BOW systems. The strongest case [41] is for Rb-TCNQ(II): its $100K$ structure has regular stacks of $TCNQ^-$ at inversion centers, negligible $\chi_M(T)$ us to $150K$ and infrared spectra that indicate broken electronic inversion symmetry. Hubbard-type models have long been used for the magnetic, optical and electrical properties of quasi-1D organic ion-radical crystals [17, 34]. The singly occupied MOs of $TCNQ^-$ form a half-filled band. The BOW phase of Hubbard-type models is narrow, close to the CDW transition. 1:1 alkali-TCNQ crystals are close [42] to the CDW transition based on their electrostatic (Madelung) energy and the electronic structure of $TCNQ^-$. The spin susceptibility of $H(x)$ is encouraging for a BOW interpretation. More quantitative modeling will require values for t, U, V and other microscopic parameters.

In summary, we have characterized the BOW phase of the linear spin-1/2 chain $H(x)$ with frustrated first and second neighbor exchange. We exploited the exact gs at $x = 1/3$ for finite N to obtain the BOW amplitude $B(1/3) = 3/8$, the magnetic gap E_m, the spectrum of low-energy excitations, and topological spin solitons between BOWs with opposite phases. The spin chain makes possible a detailed examination of a BOW phase. While quantitative results are limited to $H(x)$, the consequences of broken inversion symmetry, gs degeneracy and finite E_m hold for BOW phases in general. The spin susceptibility of $H(x)$ is consistent with the unusual $\chi_M(T)$ of alkali-TCNQ salts with regular stacks and provides additional support for the hypothesis [41] that these salts are physical realizations of BOW phases.

Acknowledgements. We thank D. Sen for valuable comments concerning the BOW phase at large J_2/J_1. ZGS thanks A. Girlando for access to unpublished RbTCNQ(II) spectra and A. Painelli for discussions about BOW systems. Princeton research was supported in part by the National Science Foundations under the MRSEC program (DMR-0819860). SR thanks DST India for funding through SR/S1/IC-08/2008 and JC Bose fellowship.

[1] M. Nakamura, Phys. Rev. B **61**, 16377 (2000);M. Nakamura, J. Phys. Soc. Jpn. **68**, 3123 (1999).

[2] P. Sengupta, A.W. Sandvik and D.K. Campbell, Phys. Rev. B **65**, 155113 (2002); K-M Tam, S-W Tsai and D.K. Campbell, Phys. Rev. Lett. 96, 036408 (2006).

[3] Y.Z. Zhang, Phys. Rev. Let. **92**, 246404 (2004).

[4] S. Glocke, A. Klumper and J. Sirker, Phys. Rev. B **76**, 155121 (2007).

[5] S. Ejima and S. Nishimoto, Phys. Rev. Lett. **99**, 216403 (2007).

[6] M. Kumar, S. Ramasesha and Z.G. Soos, Phys. Rev. B **79**, 035102 (2009).

[7] C.K. Majumdar and D.K. Ghosh, J. Math. Phys. **10**, 1399 (1969).

[8] K. Okamoto and K. Namura, Phys. Lett. A **169**, 433 (1992).

[9] B.S. Shastry and B. Sutherland, Phys. Rev. Lett. **47**, 964 (1981).

[10] I. Affleck, T. Kennedy, E.H. Lieb and H. Tasaki, Commun. Math. Phys. **115**, 477 (1988).

[11] F.D.M. Haldane, Phys. Rev. B **25**, 4925 (1982).

[12] K. Kuboki and H. Fukuyama, J. Phys. Soc. Japan **56**, 3126 (1987); T. Tonegawa and I. Harada, J. Phys. Soc. Japan **56**, 2153 (1987); I. Affleck, D. Gepner, H.J. Schultz and T. Ziman, J. Phys. A **22**, 511 (1989).

[13] R. Chitra, S. K. Pati, H. R. Krishnamurthy, D. Sen and S. Ramasesha, Phys. Rev. B **52**, 6581 (1995)

[14] S. R. White and I. Affleck, Phys. Rev. B **54**, 9862 (1996).

[15] W.P. Su, J.R. Schrieffer and A.J. Heeger, Phys. Rev. B **22**, 2099 (1980).

[16] A.J. Heeger, S. Kivelson, J.R. Schrieffer and W.P. Su, Rev. Mod. Phys. **60**, 781 (1988).

[17] Z.G. Soos, D. Mukhopadhyay, A. Painelli and A. Girlando, in *Handbook of Conducting Polymers*, Sec. Edit. (Eds. T.A. Skotheim, R. Elsenbaumer and T. Allen, Marcel Dekker, New York, P997) p. 165.

[18] S.A. Bewick and Z.G. Soos, Chem. Phys. 325, **60** (2006).

[19] J.C. Bonner and M.E. Fisher, Phys. Rev. **135**, A640 (1964).

[20] L. Hulthen, Arkiv. Mat. Astron. Fysik. **26A**, No. 11 (1938).

[21] Z.G. Soos, S. Kuwajima, and J.E. Mihalick, Phys. Rev. B **32**, 3124 (1985).

[22] M. Takahashi, J. Phys. C: Solid State Phys. **10**, 1289 (1977).

[23] S. Ramasesha and Z.G. Soos, Int. J. Quant. Chem. **25**, 1003 (1984).

[24] Z.G. Soos and S. Ramasesha, Phys. Rev. B **29**, 5410 (1984).

[25] Z.G. Soos and S. Ramasesha, in *Valence Bond Theory and Chemical Structure*, D.J. Klein and N. Trinajstic, Eds (Elsevier, Amsterdam1989), p. 81.

[26] S. Ramasesha and Z.G. Soos, in *Theoretical and Computational Chemistry*, Vol. 10, D.L. Cooper, Ed. (Elsevier, Amsterdam, 2002) p. 635.

[27] Z.G. Soos and S.A. Bewick, Chem. Phys. Lett. **421**, 210 (2006).

[28] A.E. Feiguin and S.R. White, Phys. Rev. B **72**, 220401 (R) (2005).

[29] M. Kumar, Z.G. Soos, D Sen and S. Ramasesha, unpublished.

[30] R. Bursill, G. A. Gehring, D. J. J. Farnell, J. B. Parkinson, T. Xiang, and C. Zeng, J. Phys:C **7**, 8605 (1995)

[31] Z. G. Soos and S. Ramasesha, Phys. Rev. Lett. **51**, 2374 (1983).

[32] J.S. Miller, Ed.*Extended Linear Chain Compounds*, Vol. 3 (Plenum, New York, 1983).

[33] H.T. Diep, Ed.*Frustrated Spin Systems*, (World Scientific, Hackensack, N.J. 2004).

[34] Z.G. Soos, Annu. Rev. Phys. Chem. **25**, 121 (1974); Z.G. Soos and D.J. Klein, in *Treatise on Solid State Chemistry*, Vol. III (ed. N.B. Hannay, Plenum, New York, 1976) p. 689.

[35] D.C. Johnston, R.K. Kremer, M. Troyer, X. Wang, A. Klumper, S.L. Budḱo, A.F. Panchula and P.C. Canfield, Phys. Rev. B **61**, 9558 (2000).

[36] K.-H. Mutter and P. Wielah, Z. Phys. B **100**, 619 (1996).

[37] P.G.J. van Dongen, Phys. Rev. B **49**, 7904 (1994).

[38] W.A. Seitz and D.J. Klein, Phys. Rev. B **9**, 2159 (1974).

[39] G. Juttner, A. Klumpfer and J. Suzuki, Nuclear Phys. B **522**, 471 (1998).

[40] J.G. Vegter and J. Kommandeur, Mol. Cryst. Liq. Cryst. **30**, 11 (1975).

[41] T.M. McQueen, D.M. Ho, C. Jimenez Cahua, R.J. Cava, R.A. Pascal, Jr., and Z.G. Soos, Chem. Phys. Lett. 475, **44** (2009); Z. G. Soos, M. Kumar, S. Ramasesha, and R. A. Pascal, Jr. Physica B (in press).

[42] M. Kumar, S. Ramasesha, R. A. Pascal, Jr. and Z.G. Soos, Eur. Phys. Lett. **83**, 37001 (2008).